Scientia Iranica D (2022) 29(4), 1925–1938

Sharif University of Technology
Scientia Iranica
Transactions D: Computer Science & Engineering and Electrical Engineering
http://scientiairanica.sharif.edu

A new traveling-wave-based protection algorithm based on intelligent systems

S. Hasheminejad*

Department of Electrical and Computer Engineering, Graduate University of Advanced Technology, Kerman, Iran.

Received 9 June 2019; received in revised form 1 March 2020; accepted 26 October 2020

KEYWORDS
Traveling wave;
Transmission lines protection;
Fuzzy system;
Hidden Markov model;
Teager energy operator.

Abstract. The current study proposed a novel Traveling Wave (TW)-based protection algorithm for power transmission lines using intelligent systems. This algorithm is composed of two parts: the first part of the algorithm distinguishes the internal faults from the external ones, and the other one classifies the fault types and determines the faulted phases. In this research, first, Teager Energy Operator (TEO) was employed to extract TW signals and then, Hidden Markov Model (HMM) was utilized to distinguish the internal faults from the external ones according to the output of TEO. Of note, classification of the fault types and selection of the faulted phases are two important tasks in protection algorithms. In this regard, this study presented a very accurate and robust classification algorithm based on fuzzy systems. This algorithm took into account different ratios of the modal components of the faulted current signal as the input variable of fuzzy systems. The test system was then simulated in PSCAD software and the algorithm was applied in MATLAB. Testing the proposed algorithm with a large number of test signals under different fault conditions confirmed the robustness of both algorithms in terms of internal fault and fault type classifications.

© 2022 Sharif University of Technology. All rights reserved.

1. Introduction

A powerful protection system can considerably improve the reliability of power systems. Given that new power systems are more prone to instability owing to their complicated structure, development of a fast and reliable protection system is of importance more than ever. For years, protection systems have operated based on the power frequency component, which was not fast enough in Extra High Voltage (EHV) networks [1]. In most of these methods, the relay should wait until the transient components such as DC offset and high frequency transient signals damp out. This can highly affect the protection scheme as well as the reliability of the system.

To develop high speed directional relays, Traveling Wave (TW) directional protection scheme was proposed as an alternative to the traditional scheme. In this type of protection scheme, the fault-generated high frequency components, known as disturbance in the conventional methods, are used for fault detection, fault location identification, and even fault-type classification.

In [2], the reflection coefficients of the current TWs were used to identify the fault location. An algorithm based on some methods such as four-polarity comparison, time-synchronized pilot protec-

*. *Tel.: +98 34-31623450*
E-mail address: Saeidhasheminejad@yahoo.com

doi: 10.24200/sci.2020.53731.3386

tion scheme, and high-frequency unblocking was suggested in [3] for protection of high-voltage transmission lines. In addition, a TW-based method was proposed in [4] to protect the transmission lines in the presence of renewable energies. Wavelet Transform (WT) was used in [5–7] for the extraction of TWs.

Through TW principle, some papers have attempted to identify only the direction of the fault [8]. In [8], a directional protection scheme was developed for a multi-terminal DC system equipped with an inductive DC terminal. One of the important challenges in this regard is to identify whether the fault is within the protected zone or in the external one. In this respect, the correlation matching method was used in [9] to distinguish between the internal and external faults. The algorithms presented in [8] and [9] require some information from both sides of the transmission line whose reliability depends on the reliability of the communication link. In [10], an algorithm was proposed based on a combination of WT and Principal Component Analysis (PCA) to protect the transmission lines. In this algorithm, the fault location was determined based on the time difference between the first and second TWs. Section 4 discusses the drawbacks of the mentioned algorithm. A single-ended TW-based fault-location algorithm was presented in [11] to protect the transmission lines which was based on the TW natural frequencies and a non-linear objective function constructed by TW natural frequencies. However, this algorithm may fail to function effectively in the case of high-impedance or low-inception-angle faults. TW-based algorithms are also used for the protection of the High Voltage DC (HVDC) transmission lines [12,13], inverter-dominated micro-grids [14], and distribution systems [15]. A directional relay based on the apparent surge-impedance created by the initial TWs was discussed in [16]. Here, S Transform (ST) was used in the algorithm to extract the phasor of the initial voltage and current TWs according to which the apparent surge impedance was measured. The identification of high-impedance faults was neglected in this reference. Several protection schemes were presented in [17,18] for protection of three- or multi-terminal transmission lines. In [19,20], wide-area fault-location systems were employed to protect the power systems.

Classification of the fault type and selection of the faulted phases assist the relay in choosing different algorithms to deal with different fault types. In [21], a decision-tree-based method was used for this purpose. Salehi and Namdari [22] calculated the first local modulus maxima of WT of the modal components and then, performed fault type classification and faulted phase selection based on the acquired quantities and some other numerical criteria. In [23], the fault type was classified for parallel transmission lines. Referenced studies [21–23] used numerical indices to accomplish their objectives using deterministic algorithms; however, a reliable fault type classification method was not promised. Moreover, the numerical criteria should change with a change in the protected system. In [24], a combination of TWs and fuzzy logic was considered to protect a multi-terminal HVDC system. The fault type identification process was performed in [25] using fuzzy system. In the case of the double phase to the ground faults at some inception angles, the TW amplitude of the faulted phases might be smaller than that of the healthy one due to mutual coupling among different phases. Of note, the study in [25] neglected this issue in the classification process.

Both CT and CCVT considerably affect TWs which, despite their importance [26,27], have not been taken into consideration in the previous TW-based protection algorithms.

In this regard, the current research employed a single-ended and probabilistic algorithm to distinguish between internal and external faults. In addition, it classified the fault type and selected the faulted phases. To this end, first, the sampled voltage and current signals passed through the CCVT and CT, respectively, to enter the relay. Teager Energy Operator (TEO) was then used in this paper to extract the TWs from the faulted voltage and current signals. Next, the polarity of the voltage and current TW signals were checked out to determine whether there was a forward or backward fault. In case of the presence of a forward fault, the output of TEO was modified and named as Teager Output Curve (TOC). Hidden Markov Model (HMM) was considered in the proposed algorithm to identify the internal faults from the external ones using the TOC of the input signal. HMM is a probabilistic classification algorithm that is extensively used in signal processing tasks. Finally, the fault type classification was completed using the modal components of the current signals.

The proposed algorithm in this study is considered as the first TW-based algorithm which uses a probabilistic method for the internal fault identification with no dependence on any deterministic criterion. Here, the TEO, which was used to extract TWs, is devoid of the WT drawbacks such as the complexity of computations and need for a proper mother wavelet. Its data window contains only three samples which can extract TW with acceptable resolution. The test results of the proposed algorithm based on the extensive test signals simulated by PSCAD/EMTDC software are indicative of the robustness of this algorithm whose effectiveness can be guaranteed considering the impacts of CT and CCVT as well as other factors that affect the TW signals.

2. Basic principles

2.1. TW principles

TWs are generated when a disturbance, such as a short circuit, occurs in a transmission line. They are high frequency voltage or current signals that travel from the fault point to both sides of the transmission line. The amplitude of the generated TWs significantly depends on the fault inception angle (voltage angle), fault resistance, and fault type. For a single-phase line, the initial values of the voltage and current TWs (v_1 and i_1) are as follows [10]:

$$v_1 = -\frac{Z_0}{Z_0 + 2R_f} v_f, \tag{1}$$

$$i_1 = \frac{1}{Z_0 + 2R_f} v_f = -\frac{v_1}{Z_0}, \tag{2}$$

where v_f denotes the instantaneous voltage of the fault point at the fault instant, Z_0 the wave impedance of the transmission line, and R_f the fault resistance.

The propagation speed of the TWs can be calculated through Eq. (3) [28]:

$$v = \frac{1}{\sqrt{LC}}, \tag{3}$$

where L and C are the inductance and capacitance of the distributed model of the transmission line, respectively.

When these waves reach discontinuity or a point where the line impedance changes, some of them will continue their path, while the rest reflect backward. The reflection coefficients of the voltage and current TWs are as follows [10]:

$$K_v = \frac{Z - Z_0}{Z + Z_0}, \tag{4}$$

$$K_i = -\frac{Z - Z_0}{Z + Z_0} = -K_v, \tag{5}$$

where Z is the impedance of the discontinuity point in the same direction as that of the arrived wave.

2.2. Modal transform

Phase-to-modal transform was applied to convert the dependent phases of a three-phase system into three independent components called the modal components. The Karen-Bauer phase-modal transform, suggested in this paper, can be defined through the following equation [23]:

$$\begin{pmatrix} \alpha \\ \beta \\ 0 \end{pmatrix} = \frac{1}{3} \begin{bmatrix} 1 & -1 & 0 \\ 1 & 0 & -1 \\ 1 & 1 & 1 \end{bmatrix} \begin{pmatrix} a \\ b \\ c \end{pmatrix}, \tag{6}$$

where α and β are the aerial modes, and 0 is the ground mode used to identify the grounding faults. As observed in Eq. (6), α mode shows the relationship between the two phases "a" and "b" and β mode is the relationship between the phases "a" and "c". In the process of fault type classification and faulted phase selection process, consideration of the relationship between phases "b" and "c" is essential. In this regard, a redundancy matrix is defined as Eq. (7) [23]:

$$\begin{pmatrix} \alpha \\ \beta \\ \gamma \\ 0 \end{pmatrix} = \frac{1}{3} \begin{bmatrix} 1 & -1 & 0 \\ 1 & 0 & -1 \\ 0 & 1 & -1 \\ 1 & 1 & 1 \end{bmatrix} \begin{pmatrix} a \\ b \\ c \end{pmatrix}. \tag{7}$$

2.3. Comparison of the impact of CT and CCVT on TWs

CT and CCVT, the devices used for signal measurement, are equipped with energy storage facilities in their structure. Such equipment provides a limited frequency response bandwidth for both CT and CCVT. In order to compare the impacts of CT and CCVT on the TWs, both inputs and outputs of these devices were taken into account. Figures 1 and 2 show the alpha mode of the faulted voltage and current signals before and after passing through the CCVT and CT, respectively. In addition, these figures are attributed to an Ag fault occurred at a distance of 40 km from the relay location at the fault inception time of 0.064 seconds. Of note, Ag fault confirms that phase "A" is the faulted one that is connected to the ground.

Figures 1 and 2 indicate that the frequency response bandwidth of CT is much better than that of the CCVT, as already mentioned in [29]. Therefore, it is suggested that the current TWs be incorporated into the protection algorithm.

The impact of CT is better understood while considering its frequency transfer function, as shown in Eq. (8) [26]:

$$H(s) = \frac{1 + 1.5 \times 10^{-6} S}{1 + 1.4 \times 10^{-5} S}. \tag{8}$$

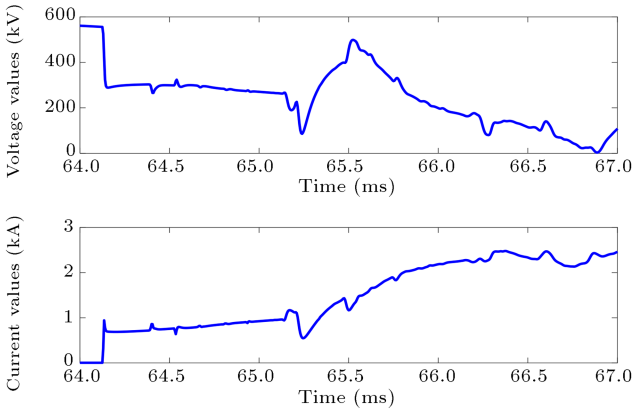

Figure 1. Alpha mode of voltage and current signals before passing through CCVT and CT.

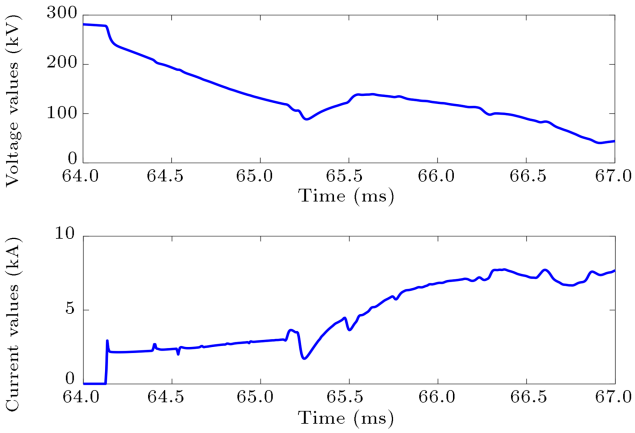

Figure 2. Alpha mode of voltage and current signals after passing through CCVT and CT.

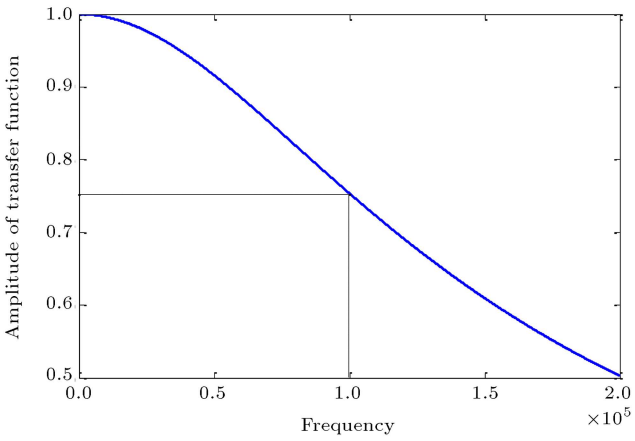

Figure 3. The magnitude of CT transfer function versus frequency.

The CT transfer function shows that at low frequencies, almost no change occurs in the frequency characteristics of the input signal. However, the amplitude of high frequency components was attenuated by CT. Figure 3 shows the magnitude of the frequency transfer function of the CT versus frequency.

In this paper, the sampling frequency was measured as 200 kHz. Therefore, according to the Nyquist theory, the frequency components up to 100 kHz can be analyzed. As observed in Figure 3, in the frequency range of 0–100 kHz, up to 25% of the frequency component amplitudes are attenuated by the CT.

3. Feature extraction and classification tools

This study employed TEO to extract TWs. In addition, it used HMM in the proposed algorithm to determine whether or not the fault is inside the protected line.

3.1. Teager Energy Operator (TEO)

TEO is a nonlinear signal operator that was first developed by Teager and Teager [30]. Then, Kaiser [31] suggested the application of this operator in extracting the energy of a specified signal. More details about the TEO functions were provided in [32].

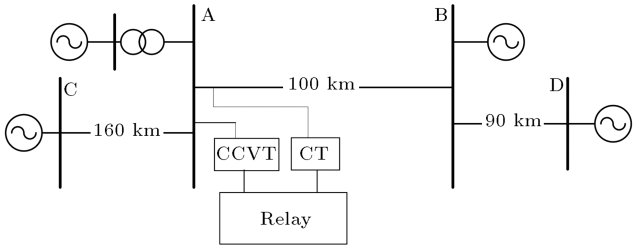

Figure 4. Single line diagram of the simulated test system.

3.2. Hidden Markov Model (HMM)

HMM is a probabilistic method which is commonly used in the classification processes. It contains two different stages of testing and training. In the training stage, HMM blocks should be trained by an adequate number of train signals. In the testing stage, an unidentified signal enters all HMM blocks and the Maximum Likelihood Probability (MLP) for each block is determined. The input signal belongs to the HMM block with the greatest MLP. For example, two HMM blocks are trained here: one for the faults along in the protected line and the other for the faults outside the protected line. As a result, both internal and external faults can be distinguished from each other. More details about the HMM formulations were given in [33,34]. Section 4.2.2 elaborates the HMM application in this study.

4. The proposed algorithm

Figure 4 presents the power system which is considered as the test system where line AB is the protected line.

Deterministic methods as well as the algorithm presented in [10] consider the time difference between the first and second TWs, hence not reliable enough. There are two different faults given in Figure 4: One is 20 km from the relay point in line AB and the other is 20 km from bus B in line BD. As shown in Figure 5, the time difference between the first and second TWs, arriving at the relay location, is just the same. Therefore, the algorithm may cause a wrong action here.

In this research, the internal and external faults were first distinguished from each other and then, the fault location was identified in two sections of signal preparation and classification process.

4.1. The identification of forward and backward faults

Karen-Bauer modal components were used to identify the forward and backward faults. The first TW was extracted from both voltage and current signals. The

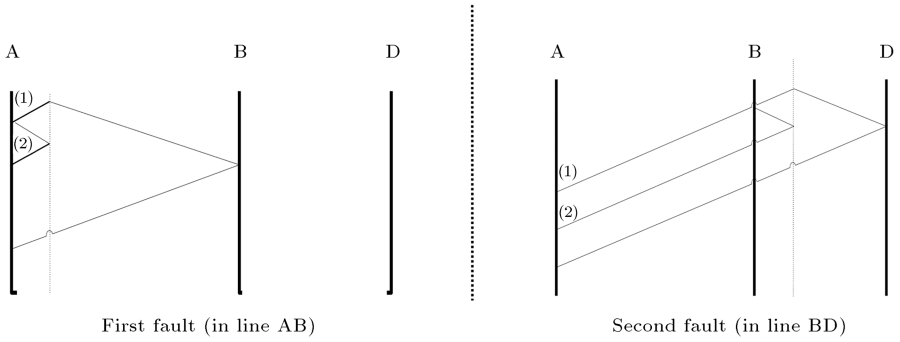

Figure 5. Lattice diagram for the two mentioned faults.

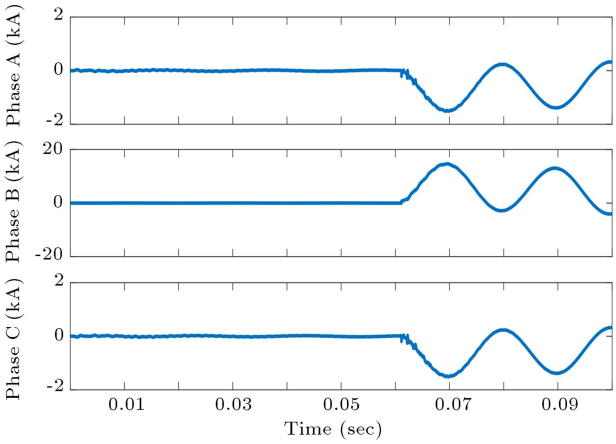

Figure 6. Three phase faulted current signals.

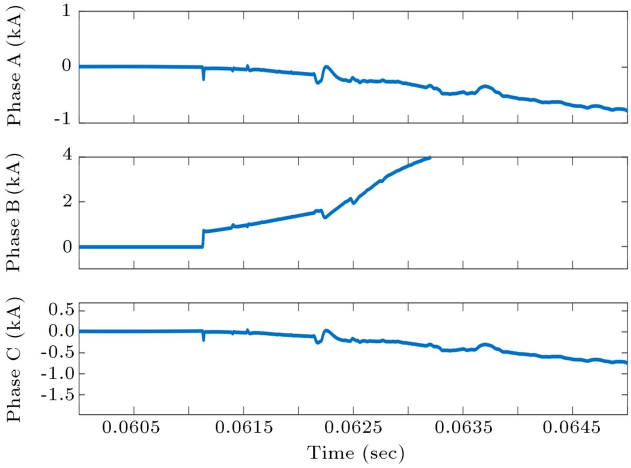

Figure 7. The magnified three phase current signals.

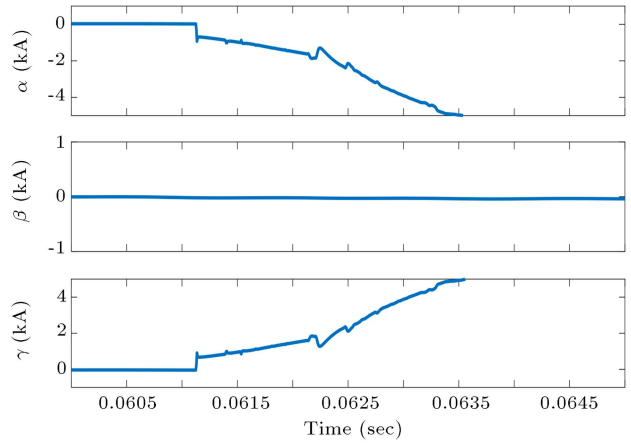

Figure 8. Modal components of the phase currents shown in Figure 7.

first voltage and current TWs are represented by Δv and Δi, respectively. If Δv is assumed to be a rise in the voltage signal, then it is positive; otherwise, it is negative. If Δi is assumed to be a rise in the current signal, it is positive; otherwise, it is negative. Based on Eq. (14), one can conclude that the faulted signals are related to either a forward or backward fault.

$$Forward\ fault: \Delta i \times \Delta v < 0,$$

$$Backward\ fault: \Delta i \times \Delta v > 0. \quad (9)$$

4.2. Identifying internal and external faults

Followed by detecting a forward fault, it should be determined whether or not the fault is inside the protected line. Figure 6 shows the three phase current signals related to a single phase to ground (Bg) fault that occurred 40 km away from the relay location. The fault inception time is 0.061 seconds, and the fault resistance in 0 Ω.

In order to better show the TW signals, the current signals between times 0.06 and 0.065 seconds are magnified, as shown in Figure 7. The respective modal components are listed in Figure 8.

4.2.1. Signal preparation

Applying TEO: In order to extract TWs, TEO was applied to the modal components of the current signal. Figure 9 shows the alpha mode of the faulted current signal given in Figure 8 as well as the obtained TEO result.

TOC generation: The TEO output should be prepared to be used for training HMM blocks. In this regard, the peaks related to the TEO outputs were extracted to form TOC. Note that a combination of one rise and one fall is regarded as one peak. Each point in TOC

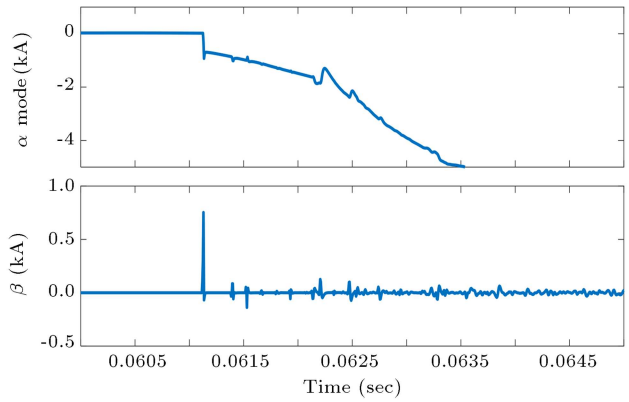

Figure 9. (a) Typical current TW signals and (b) their TEO result.

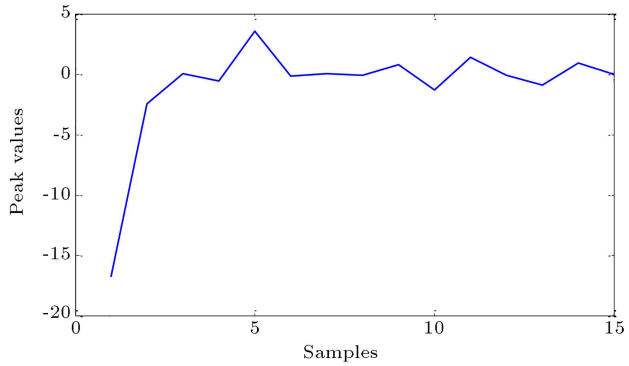

Figure 10. TOC of the signal in Figure 9.

is related to a peak in the TEO result. The first 15 peaks of the TEO result are considered to form the TOC. Figure 10 shows the TOC of the signal shown in Figure 9.

Scaling process: Fault impedance and fault inception angle affect the magnitude of the TWs. However, these factors should not undermine the performance of the algorithm. The only thing that should be different for the internal and external faults is where the successive TWs are reflected or transmitted from. Therefore, TWs are scaled between 0 and 1. The formulation is given below:

$$k_y = 1/(y_{\max} - y_{\min}), \tag{10}$$

$$y' = y - y_{\min}, \tag{11}$$

$$y_{new} = k_y y', \tag{12}$$

where $y_{\min}$ and $y_{\max}$ are the minimum and maximum values of the TOC, respectively, and "y" indicates each point of TOC.

4.2.2. Classification process

In the case of fault occurrence, TOC of the faulted current signal was analyzed by HMM. HMM can discriminate between the TOCs of the internal and external faults. The difference between the two sets of patterns comes from the difference between the reflection coefficients of the buses with which TWs are facing.

HMM has two different stages of training and testing. These stages are as follows:

Training stage: In this stage, two different HMM blocks are trained. The first HMM block is trained by adequate numbers of TOCs related to the internal faults and those related to the external faults were employed to train the second HMM block. In this respect, different internal and external faults with different fault locations, impedance, and inception angles were taken into account. Figure 11 shows the TOC of the α modal current signal of a typical internal fault and a typical external fault, respectively.

As observed in Figures 11 and 12, the most prominent difference between these two signals, i.e., the difference between the magnitude of the first TW and that of the next ones, is greater for the internal faults than for the external faults, mainly because the first TW experienced no refraction but the TW of the external fault was refracted while passing bus B in Figure 4. Moreover, the successive reflections were different in the internal and external faults. The result of the training process generates two matrices for each HMM block characterized by one transmission matrix and an emission matrix.

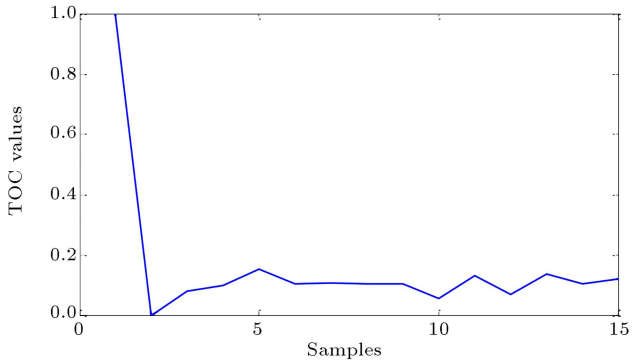

Figure 11. TOC related to the internal fault.

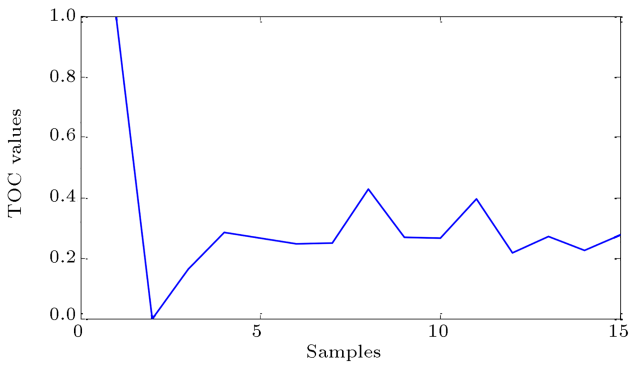

Figure 12. TOC related to the external fault.

Testing stage: In order to ensure protection for the protected lines, TEO was applied to the line current signal. The data window of TEO contains three samples. When a fault occurs, the generated TWs are detected based on the TEO results. After detecting 15 successive TWs, TOC is generated. Then, the scaling process is performed. The resulting curve is entered into both HMM blocks, and the MLP is calculated for each HMM one. The generated MLP of the internal and the external fault HMM blocks is indicative of a similarity of the TOC of the test signal to that of each of the internal and external faults, respectively. If the MLP related to the internal fault HMM block is higher than its counterpart, the test signal is classified as an internal fault and the relay trips the line. Otherwise, the test signal is classified as an external fault.

4.3. Fault classification and faulted phases selection

The initial current TW, extracted by TEO, was used for fault type classification and faulted phase selection. Of note, the modal components of the current signals were used in this process. Then, a proper fuzzy system was utilized to determine the fault type.

The magnitude of the TW depends on the fault inception angle and fault impedance. In order to nullify the impact of these parameters, it is recommended to consider the ratios of the modal components (I_α/I_β, I_α/I_γ, I_β/I_γ) in the decision-making process. Here, I_α, I_β, and I_γ are the amplitudes of the initial current TW of alpha, beta, and gamma modes, respectively. For each of these fault types, the ratio of the first TW amplitude of the zero sequence to the maximum of that of the three modal components (which is called zero-ratio here) is considered to identify grounded faults from ungrounded ones. Table 1 presents the results of extensive experiments at all possible fault inception angles, different fault impedances, and different fault distances for different fault types.

Further experiments were then carried out to discriminate between the double phase to the ground faults. According to Table 1 and further analysis of double phase to the ground faults, it can be concluded that:

When zero-ratio $> 10^{-5}$:

- If $0.95 < \frac{I_\alpha}{I_\beta} < 1.05$ and $100 < \frac{I_\alpha}{I_\gamma} < 2 \times 10^6$ and $100 < \frac{I_\beta}{I_\gamma} < 2 \times 10^6$, then Ag fault is concluded;
- If $100 < \frac{I_\alpha}{I_\beta} < 2 \times 10^6$ and $0.95 < \frac{I_\alpha}{I_\gamma} < 1.05$ and $10^{-7} < \frac{I_\beta}{I_\gamma} < 0.005$, then Bg fault is concluded;
- If $10^{-7} < \frac{I_\alpha}{I_\beta} < 0.005$ and $10^{-7} < \frac{I_\alpha}{I_\gamma} < 0.005$ and $0.95 < \frac{I_\beta}{I_\gamma} < 1.05$, then Cg fault is concluded;
- Otherwise, a double phase to ground fault is concluded.

When zero-ratio $< 10^{-5}$:

- If $3.5 < \frac{I_\alpha}{I_\beta} < 4.5$ and $3.5 < \frac{I_\alpha}{I_\gamma} < 4.5$ and $0.95 < \frac{I_\beta}{I_\gamma} < 1.05$, then AB fault is concluded;
- If $0.2 < \frac{I_\alpha}{I_\beta} < 0.3$ and $0.95 < \frac{I_\alpha}{I_\gamma} < 1.05$ and $3.5 < \frac{I_\beta}{I_\gamma} < 4.5$, then AC fault is concluded;
- If $0.95 < \frac{I_\alpha}{I_\beta} < 1.05$ and $0.2 < \frac{I_\alpha}{I_\gamma} < 0.3$ and $0.2 < \frac{I_\beta}{I_\gamma} < 0.3$, then BC fault is concluded;
- Otherwise, a three-phase fault is concluded.

When there is a double phase to the ground fault phase:

- If $10^{-5} <$ zero-ratio < 0.16 and $\frac{I_\alpha}{I_\beta} > 1$ and $\frac{I_\alpha}{I_\gamma} > 1$, then ABg fault is concluded;

Table 1. Values of selected parameters for different fault types.

	Zero-ratio	I_α/I_β	I_α/I_γ	I_β/I_γ
Ag	$0.1 \sim 0.9$	$1 \sim 1.02$	$150.3 \sim 1.5 \times 10^6$	$148 \sim 1.5 \times 10^6$
Bg	$0.1 \sim 0.9$	$150.3 \sim 1.5 \times 10^6$	$1 \sim 1.02$	$6.5 \times 10^{-7} \sim 6.6 \times 10^{-3}$
Cg	$0.1 \sim 0.9$	$6.5 \times 10^{-7} \sim 6.6 \times 10^{-3}$	$6.5 \times 10^{-7} \sim 6.6 \times 10^{-3}$	$1 \sim 1.02$
AB	$1.2 \times 10^{-10} \sim 6 \times 10^{-8}$	$3.9 \sim 4.1$	$3.9 \sim 4.1$	$0.97 \sim 1.01$
AC	$1.2 \times 10^{-10} \sim 6 \times 10^{-8}$	$0.24 \sim 0.25$	$0.97 \sim 1.01$	$3.9 \sim 4.1$
BC	$1.2 \times 10^{-10} \sim 6 \times 10^{-8}$	$0.97 \sim 1.01$	$0.24 \sim 0.25$	$0.24 \sim 0.25$
ABg	$0.0021 \sim 1.0773$	$0.1 \sim 22.7$	$0.01 \sim 42.6$	$0.05 \sim 42.1$
ACg	$0.0021 \sim 1.0773$	$0.02 \sim 49.1$	$0.02 \sim 18.3$	$0.02 \sim 23.1$
BCg	$0.0021 \sim 1.0773$	$0.04 \sim 32.6$	$0.03 \sim 46.9$	$0.04 \sim 27.3$
ABCg	$9.77 \times 10^{-9} \sim 5.8 \times 10^{-7}$	$0.002 \sim 712$	$0.002 \sim 2.6 \times 10^3$	$0.001 \sim 2.6 \times 10^3$

- If 10^{-5} < zero-ratio < 0.16 and $\frac{I_\alpha}{I_\beta} < 1$ and $\frac{I_\beta}{I_\gamma} > 1$, then ACg fault is concluded;
- If 10^{-5} < zero-ratio < 0.16 and $\frac{I_\alpha}{I_\gamma} < 1$ and $\frac{I_\beta}{I_\gamma} < 1$, then BCg fault is concluded;
- If 0.16 < zero-ratio< 0.37 and ($\frac{I_\alpha}{I_\beta} > 1$ and $\frac{I_\alpha}{I_\gamma} < 1$ or vice versa), then ABg fault is concluded;
- If 0.16 < zero-ratio< 0.37 and ($\frac{I_\alpha}{I_\beta} > 1$ and $\frac{I_\beta}{I_\gamma} < 1$ or vice versa), then ACg fault is concluded.
- If 0.16 < zero-ratio< 0.37 and ($\frac{I_\alpha}{I_\gamma} > 1$ and $\frac{I_\beta}{I_\gamma} < 1$ or vice versa), then BCg fault is concluded;
- If 0.37 < zero-ratio and $\frac{I_\alpha}{I_\beta} < 1$ and $\frac{I_\alpha}{I_\gamma} < 1$, then ABg fault is concluded;
- If 0.37 < zero-ratio and $\frac{I_\alpha}{I_\beta} > 1$ and $\frac{I_\beta}{I_\gamma} < 1$, then ACg fault is concluded;
- If 0.37 < zero-ratio and $\frac{I_\alpha}{I_\gamma} > 1$ and $\frac{I_\beta}{I_\gamma} > 1$, then BCg fault is concluded.

According to Table 1 and gathered rules for the proposed algorithm, there are two Sugeno-based fuzzy systems with four variables. Each variable has its specific membership functions. Table 2 lists four variables and their related membership functions.

In the first fuzzy system, Ag, Bg, Cg, AB, AC, BC, double phase to ground and three-line faults are distinguished from each other and their fuzzy output indexes are 1 to 8, respectively. Double phase to ground faults (ABg, ACg, and BCg) are distinguished from each other through the second fuzzy system. The output indices of the second fuzzy system are 1, 2, and 3 which are related to ABg, ACg, and BCg, respectively.

Figure 13 shows the flowchart of the proposed algorithm. Figures 14 and 15 present the internal fault identification and fault type classification blocks.

5. Simulation and results

In order to demonstrate the feasibility of the application of the proposed algorithm, different testing and training signals were generated by PSCAD/EMTDC software, and the rest of the protection algorithms were implemented by MATLAB. In this regard, a 400 kV transmission network was simulated in PSCAD software, and the data were generated at a sampling frequency of 200 kHz. A saturable 1600A/5A CT with a flux density of 1 Tesla on its knee point was also utilized to extract the current signals. The CCVT of the system was wrought by two capacitors and a voltage transformer. The overall transformation ratio for CCVT was calculated as 231×10^3 V/115V.

5.1. Internal fault identification

A large number of internal and external faults were generated through the simulated system. Then, the TOC of each signal was generated and used in the training process. Fault distance, fault inception angle, and fault impedance were changed to generate different internal and external faults. The fault distance from the relay location for the internal and external faults was changed from 2 km to 98 km and 102 km to 188 km, respectively. In addition, the fault inception angle and

Table 2. Variables and membership functions for fault classification and faulted phases selection algorithm.

	$\frac{I_0}{\max(I_\alpha, I_\beta, I_\gamma)}$	I_α/I_β	I_α/I_γ	I_β/I_γ
MF type	Trapezoidal	Trapezoidal	Trapezoidal	Trapezoidal
MF_1	$-0.01, 0,$ $10^{-5}, 2 \times 10^{-5}$	$-0.01, 0,$ $0.1, 0.12$	$-0.01, 0,$ $0.1, 0.12$	$-0.01, 0,$ $0.1, 0.12$
MF_2	$10^{-5}, 5 \times 10^{-5},$ $0.9, 1$	$0.1, 0.12,$ $0.8, 0.9$	$0.1, 0.12,$ $0.8, 0.9$	$0.1, 0.12,$ $0.8, 0.9$
MF_3	–	0.8, 0.9, 1.8, 2	0.8, 0.9, 1.8, 2	0.8, 0.9, 1.8, 2
MF_4	–	1.8, 2, 5, 5.5	1.8, 2, 5, 5.5	1.8, 2, 5, 5.5
MF_5	–	$90, 100, 2 \times 10^6,$ 2.5×10^6	$90, 100, 2 \times 10^6,$ 2.5×10^6	$90, 100, 2 \times 10^6,$ 2.5×10^6

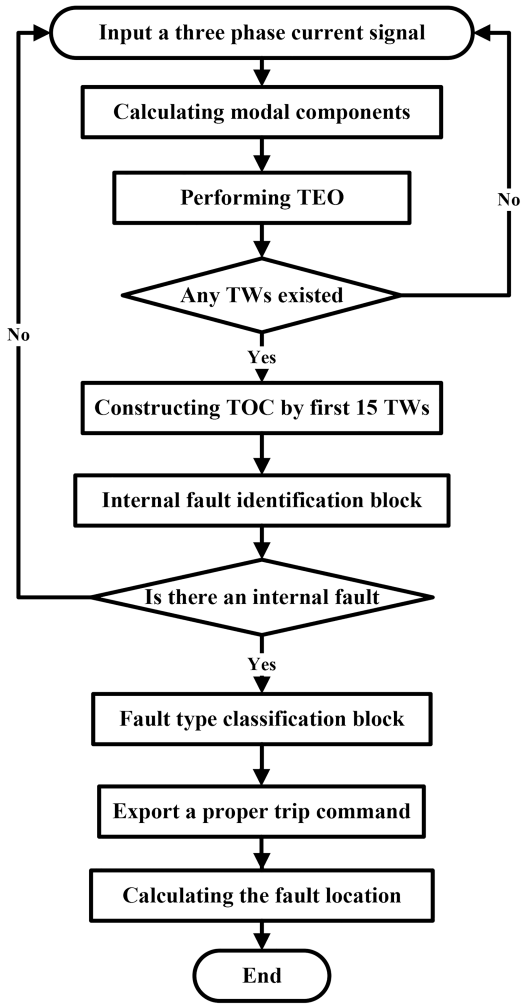

Figure 13. Flowchart of the proposed algorithm.

Table 3. Simulation results for the internal fault identification.

	Ag	AC	BCg	ABC
Inception angle	48 deg	90 deg	36 deg	120 deg
R	5 Ω	10 Ω	0.01 Ω	1 Ω
Distance	10 km	50 km	30 km	70 km
MLP_internal	–19.05	–25.07	–312.33	–13.62
MLP_external	–19.19	–31.64	–695.96	–1136.2

fault impedance for both internal and external faults were changed from 2 to 178 degrees and from 0 to 50 Ω, respectively. Different fault types were considered in the train signals. Faulted signals that are different from the train signals are commonly used to assess the performance of the proposed algorithm. Table 3 shows some of the obtained results.

According to the results, the MLP of the internal fault HMM block was greater than that of the external fault. For example, an AC internal fault with the fault inception angle of 90 degrees and fault resistance of 10 Ω in the middle of the transmission line is observed in the third column of Table 3. Here, the MLPs of the external and internal faults were measured as –31.64 and –25.07, respectively. Obviously, the MLP of the internal fault is greater than that of the external fault; for this reason, the fault is considered internal.

5.2. External fault identification

In order to evaluate the performance of the proposed algorithm, the external faults were simulated and used as the test signals. Table 4 shows the results of the proposed algorithm to identify the external faults.

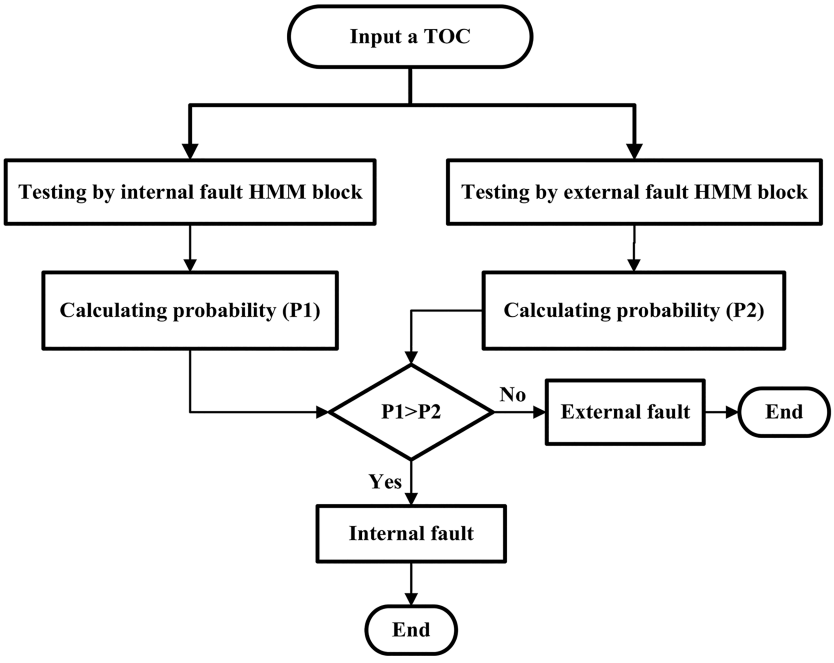

Figure 14. Internal fault identification block.

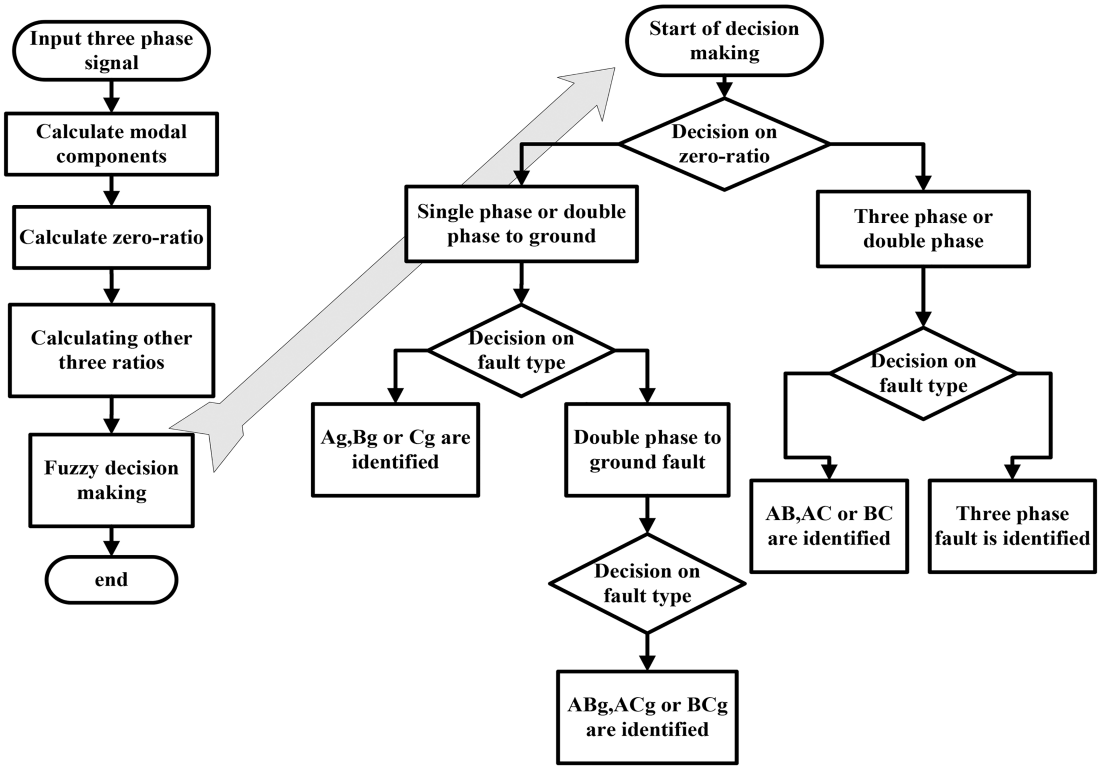

Figure 15. Fault type classification block.

Table 4. Simulation results for the external fault identification.

	Bg	AB	ACg	ABCg
Inception angle	45 deg	90 deg	60 deg	135 deg
R	5 Ω	10 Ω	0.01 Ω	1 Ω
Distance	120 km	130 km	140 km	150 km
MLP_internal	–30.4	–30.14	–65.22	–29.15
MLP_external	–24.7	–29.86	–40.72	–28.27

The results also indicate that the proposed algorithm can accurately identify the external faults and prevent the relay from sending a trip command for them.

5.3. The identification of high-impedance faults

To investigate the impact of high-impedance faults on the performance of the proposed algorithm, some high-impedance faults are considered whose current signals are used as the test signals for the proposed algorithm. Table 5 shows the results of testing the proposed algorithm with high-impedance faults.

According to Table 5, the proposed algorithm exhibited appropriate performance in case of high-impedance faults.

5.4. The impact of close-in faults

To ensure the proper performance of the proposed algorithm, the close-in faults were investigated. Table 6 shows the results of identifying the close-in faults using the proposed algorithm.

Table 5. Simulation results for high-impedance faults.

	Bg	AC	BC	ABg
Inception angle	30 deg	120 deg	70 deg	90 deg
R	50 Ω	30 Ω	5 Ω	30 Ω
Distance	70 km	50 km	90 km	30 km
MLP_internal	–23.99	–18.30	–22.71	–29.71
MLP_external	–43.40	–19.06	–23.86	–41.91

Table 6. Performance of the proposed algorithm face with close-in faults.

	Ag	BC	BCg	ABCg
Inception angle	45 deg	90 deg	30 deg	60 deg
R	0.01 Ω	10 Ω	0.01 Ω	10 Ω
Distance	2 km	2 km	5 km	5 km
MLP_internal	–20.84	–39.07	–18.87	–139.63
MLP_external	–110.76	–88.32	–21.66	–631.74

5.5. Low inception angle faults

Low inception angle faults are faults whose phase voltage value is close to zero. For these faults, the amplitude of the generated TWs is quite low which can be considered a challenge for the TW-based protection

Table 7. Simulation results for low inception angle faults.

	Ag	Cg	AB	AC
Inception angle	5 deg	65 deg	155 deg	35 deg
R	0.01 Ω	0.01 Ω	0.01 Ω	0.01 Ω
Distance	40 km	40 km	40 km	40 km
MLP_internal	–29.65	–36.16	–17.45	–28.80
MLP_external	–34.48	–37.86	–31.73	–40.39

algorithms. To evaluate the performance of the proposed algorithm in case of low inception angle faults, some of these faults were simulated and used as the test signals, the results of which are given in Table 7.

According to Table 3, the low inception angle for a Cg fault is 65 degrees. Assume that the zero-crossing of phase "A" is 0. Then, the zero-crossing of phase "C" becomes 60 degrees. The low inception angle for an AC fault is 35 degrees. Since the amplitudes of the TWs are quite low for a double-phase fault and the voltage values of the two faulted phases are equal, the corresponding angle for an AC fault is 30°.

5.6. Fault classification and faulted phase selection

A large number of test signals were used to evaluate the performance of the proposed algorithm in terms of fault type classification and faulted phase selection. These signals were generated by changing the inception angle, impedance, and location of the faults. The results from fault classification highlighted the ability of the proposed method to appropriately classify all faults, hence the highest possible accuracy. Some of the related results are given in Table 8 where the outputs of the first fuzzy system are indices from 1 to 8, corresponding to Ag, Bg, Cg, AB, AC, BC, double phase to ground faults, and three-phase faults, respectively. The outputs of the second fuzzy system are indices from 1 to 3 represented for ABg, ACg, and BCg faults, respectively.

Consider the AC fault in the third column of Table 8. The value of the zero ratio shows that the fault is not grounded. The values of I_α/I_β, I_α/I_γ, and I_β/I_γ show that phases A and C are the two faulted phases.

5.6.1. Classification of high-impedance faults

The proposed classification algorithm should work appropriately when facing faults with any impedance. As a result, faults of high resistance are generated, and the TWs in their current signals are used as the test signals for the proposed classification algorithm. Table 9 shows the obtained results in this regard.

Table 9 emphasizes the capability of the proposed classification algorithm to accurately classify high-impedance faults. For example, as observed in the last column of this table, the value of zero-ratio is indicative of the presence of a grounded fault. Moreover, accord-

Table 8. Simulation results for the classification algorithm.

	Ag	AC	BCg	ABCg
Inception angle	36 deg	36 deg	45 deg	90 deg
R	1 Ω	10 Ω	0.01 Ω	1 Ω
Distance	30 km	30 km	7 km	5 km
I_α/I_β	1.01	0.252	17.4835	5.9929
I_α/I_γ	1.7×10^6	1.0161	0.6512	2.8583
I_β/I_γ	1.7×10^6	4.0323	0.0372	0.4769
Zero-ratio	0.1277	6.5×10^{-10}	0.2384	1.2×10^{-7}
Fuzzy index	1	5	7,3	8

Table 9. Results of the classification algorithm for high resistance faults.

	Bg	BC	ABg	BCg
Inception angle	36 deg	36 deg	36 deg	36 deg
R	50 Ω	50 Ω	50 Ω	50 Ω
Distance	30 km	30 km	30 km	30 km
I_α/I_β	2.5×10^6	0.9802	4.5048	8.332
I_α/I_γ	0.9878	0.2475	3.5758	0.6728
I_β/I_γ	3.9×10^{-7}	0.2525	0.7938	0.0807
Zero-ratio	0.1261	3.3×10^{-10}	3.4×10^{-10}	0.0531
Fuzzy index	2	6	7, 1	7, 3

Table 10. Simulation results for the classification of close-in faults.

	Ag	**AC**	**BCg**	**ABCg**
Inception angle	36 deg	36 deg	36 deg	36 deg
R	0.01 Ω	1 Ω	0.01 Ω	1 Ω
Distance	3 km	3 km	3 km	3 km
I_α/I_β	1.0064	0.2513	10.5532	6.1099
I_α/I_γ	2.6×10^6	1.0105	0.5851	2.8205
I_β/I_γ	2.6×10^6	4.021	0.0554	0.4616
Zero-ratio	0.8132	3.3×10^{-10}	0.2353	1.1×10^{-7}
Fuzzy index	1	5	7,3	8

Table 11. Simulation results for low inception angle faults.

	Cg	**AB**	**BC**	**ACg**
Inception angle	65 deg	125 deg	95 deg	35 deg
R	1 Ω	0.01 Ω	5 Ω	10 Ω
Distance	20 km	40 km	60 km	80 km
I_α/I_β	4.24×10^{-5}	3.97	0.254	2.112
I_α/I_γ	4.37×10^{-5}	4.02	1.03	8.83
I_β/I_γ	1.03	1.013	4.06	4.18
Zero-ratio	0.0157	5×10^{-9}	3×10^{-9}	0.2284
Fuzzy index	3	4	6	7,2

ing to the values of other ratios and the fuzzy rules, the existence of a BCg fault can be proved.

5.6.2. Classification of close-in faults

Table 10 shows the performance of the proposed classification algorithm in terms of the classification of the close-in faults.

5.6.3. Classification of low-inception-angle faults

The proposed classification algorithm is able to effectively classify the faults with low inception angle. To this end, different faults with low inception angles were taken into consideration, as shown in Table 11.

5.7. The impact of noise on the algorithms

In order to evaluate the performance of the proposed algorithms in noisy conditions, some random noises were added to the test signals. Figure 16 shows the alpha mode of the contaminated signal and its TEO output. The signal is attributed to an AB fault with the fault inception angle of 65 degrees and fault resistance of 0.01 Ω occurring 40 km away from the relay location. Here, the outputs of the internal and external fault HMM blocks were calculated as –120.71 and −838.13, respectively. Therefore, the faulted signal is classified as an internal fault.

The faulted current signals are used as the test signals for the fault type classification and faulted phase selection. In this process, $\frac{I_\alpha}{I_\beta} = 3.896$, $\frac{I_\alpha}{I_\gamma} = 4.107$, $\frac{I_\beta}{I_\gamma} = 1.054$, and zero-ratio = 0.001. These parameters are used as the input of the fuzzy system. The output index of the fuzzy system is 4, indicating the existence of an AB fault.

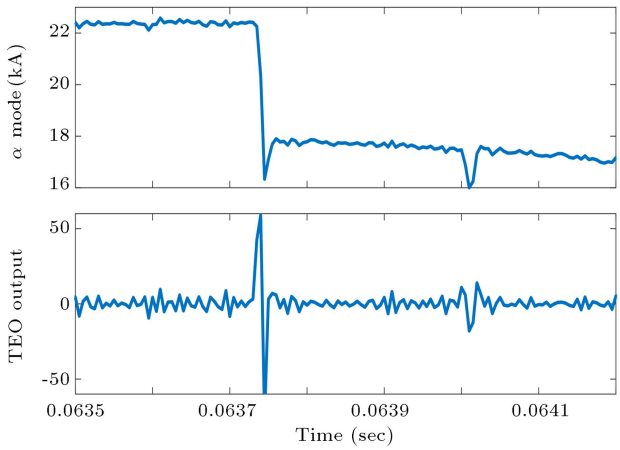

Figure 16. Noisy current signal and its TEO output.

6. Conclusion

The algorithms proposed in this research can highly improve the Traveling Wave (TW)-based protection of transmission lines. In this regard, Teager Energy Operator (TEO) as an easy method could effectively extract TWs with high resolution and low mathemat-

ical calculations. For the internal fault identification, application of a probabilistic method (HMM) instead of deterministic algorithms would lead to establishment of a much more reliable method characterized by different networks and fault situations. Deterministic algorithms use a limited number of criteria for internal fault identification or fault type classification. On the contrary, intelligent algorithms are multi-criteria in nature, hence more reliable for engineering applications. It should be mentioned that consideration of the ratios of the initial current TWs of the modal components along with a fuzzy system made the proposed classification algorithm fast and accurate, thus enabling it to make correct decisions in any given fault situation.

References

1. Masoud, M.E. and Mahfouz, M.M.A. "Protection scheme for transmission lines based on alienation coefficients for current signals", *IET Gener. Transm. Distrib.*, **4**(11), pp. 1236–1244 (2010).
2. Sawai, S. and Pradhan, A.K. "Traveling-wave-based protection of transmission line using single-end data", *IET Gener. Transm. Distr.*, **13**(20), pp. 4659–4666 (2019).
3. Li, Y., Wang, J., and Liu, K. "Improved travelling wave protection for extra-high-voltage/ultra-high-voltage transmission lines", *Jour. of Eng.*, **2019**(16), pp. 3280–3283 (2019).
4. Aftab, M.A., Hussain, S.M., Ali, I., et al. "Dynamic protection of power systems with high penetration of renewable: A review of travelling wave based fault location technique", *Int. Jour. Elect. Power & Ener. Syst.*, **11**(4), pp. 1–13 (2020).
5. Jena, S. and Bhalja, B.R. "Initial travelling wave front-based bus zone protection scheme", *IET Gener. Trans. & Distrib.*, **13**(15), pp. 3216–3229 (2019).
6. Liang, H., Liu, Y., Sheng, G., et al. "Inversion method to reconstruct fault transient traveling wave on overhead transmission lines", *Int. Trans. Elect. Energy Syst.*, **28**(6), pp. 1–21 (2018).
7. Sharafi, A., Sanaye-Pasand, M., and Jafarian, P. "Improvement of distance relay zone-3 security using fault and breaker opening generated traveling waves", *Int. Trans. Elect. Energy Syst.*, **27**(10), pp. 1–12 (2017).
8. Li, Y., Gong, Y., and Jiang, B. "A novel traveling-wave-based directional protection scheme for MTDC grid with inductive DC terminal", *Elect. Power Syst. Res.*, **15**(7), pp. 83–92 (2018).
9. Zhang, G., Shu, H., and Liao, Y. "Automated double-ended traveling wave record correlation for transmission line disturbance analysis", *Elect. Power Syst. Res.*, **13**(6), pp. 242–250 (2016).
10. Jafarian, P. and Sanaye-Pasand, M. "A traveling-wave-based protection technique using wavelet/PCA analysis", *IEEE Trans. Power Del.*, **25**(2), pp. 588–599 (2010).
11. He, Z., Li, X., and Chen, S. "A traveling wave natural-frequency-based single-ended fault location method with unknown equivalent system impedance", *Intern. Trans. Elect. Ener. Syst.*, **26**(3), pp. 509–524 (2016).
12. Zheng, J., Wen, M., Qin, Y., et al. "A novel pilot directional backup protection scheme based on transient current for HVDC lines", *Intern. Jour. Elect. Ener. Syst.*, **11**(5), Article 105424 (2020).
13. Wang, D., Hou, M., Gao, M., et al. "Travelling wave directional pilot protection for hybrid HVDC transmission line", *Inter. Jour. Elect. Power Ener. Syst.*, **10**(7), pp. 615–627 (2019).
14. Li, X., Dysco, A., and Burt, G.M. "Traveling-wave-based protection scheme for inverter-dominated microgrid using mathematical morphology", *IEEE Trans. Smart Grid*, **5**(2), pp. 2211–2218 (2014).
15. Elkalashy, N.I., Sabiha, N.A., and Lehtonen, M. "Earth fault distance estimation using active traveling waves in energized compensated MV networks", *IEEE Trans. Power Del.*, **30**(2), pp. 836–843 (2015).
16. He, Z., Liu, X., Li, X., et al. "A novel traveling wave directional relay based on apparent surge impedance", *IEEE Trans. Power Del.*, **30**(3), pp. 2253–2261 (2015).
17. Khodadadi, M. and Shahrtash, S.M. "A new non-communication-based protection scheme for three-terminal transmission lines employing mathematical morphology-based filters", *IEEE Trans. Power Del.*, **28**(2), pp. 347–356 (2013).
18. Livani, H. and Yaman, C. "A fault classification and localization method for three-terminal circuits using machine learning", *IEEE Trans. Power Del.*, **28**(4), pp. 2282–2290 (2013).
19. Li, Z., Cheng, Y., Wang, X., et al. "Study on widearea traveling wave fault line selection and fault location algorithm", *Int. Trans. Elec. Energy Syst.*, **28**(12), pp. 1–13 (2018).
20. Salehi-Dobakhshari, A. and Ranjbar, A.M. "Application of synchronized phasor measurements to wide-area fault diagnosis and location", *IET Gener. Transm. Distrib.*, **8**(4), pp. 716–729 (2014).
21. Hasheminejad, S., Seifossadat, S.G., Razaz, M., et al. "Ultra-high-speed protection of transmission lines using traveling-wave theory", *Elec. Power Syst. Res.*, **13**(2), pp. 94–103 (2016).
22. Salehi, M. and Namdari, F. "Fault classification and faulted phase selection for transmission line using morphological edge detection filter", *IET, Gener. Transm. Distr.*, **12**(7), pp. 1595–1605 (2018).
23. Hasheminejad, S., Seifossadat, G.H., Razaz, M., et al. "Traveling-wave-based protection of parallel transmission lines using Teager energy operator and fuzzy systems", *IET Gener. Transm. Distrib.*, **10**(4), pp. 1067–1074 (2016).
24. Hessam-Eldin, A., Lofti, A., Elgamal, M., et al. "Combined traveling wave and fuzzy logic based fault location in multi-terminal HVDC system", *16TH intern. Conf. on Environ. Electr. Eng.* (2016).

25. AbulKalam, M. and Jamil, M. "Wavelet-fuzzy based protection scheme of EHV-AC transmission system and efficacy of discrete Fourier transform", *Jour. Elect. Syst. And Inf. Tech.*, **5**(3), pp. 371–387 (2018).

26. Yonghong, T., Wei, Z., Zhen, H., et al. "Study on effect of current transformer and its secondary cable to traveling wave propagation characteristic of electric power lines", *Int. Conf. Intel. Sys. Design and Eng. App., Sanya, Hainan*, pp. 1495–1598 (2012).

27. Sefidpour, S., Wang. J., and Srivastava, K. "Factors affecting traveling wave protection", *The Int. Conf. Adv. Power Sys. Automandprot.*, China, pp. 1359–1365 (2011).

28. Akmaz, D., Mamis, M.S., Arkan, M., et al. "Transmission line fault location using traveling wave frequencies and extreme learning machine", *Elect. Power Syst. Res.*, **15**(5), pp. 1–7 (2018).

29. Dong, X., Luo, S., Shi, S., et al. "Travelling wave based directional comparison protection scheme and its application in 750 kV transmission lines", *IEEE Power & Ener. Soc.* (2015).

30. Teager, H.M. and Teager, S.M. "Evidence for nonlinear sound production mechanisms in vocal tract, In speech production and modeling speech production and speech modeling", *NATO ASI Series*, **5**(5), pp. 241–261 (1990).

31. Kaiser, J.F. "Some useful properties of Teager's energy operator", In *Proc. ICASSP-93*, **3**, pp. 149–152 (1993).

32. Hasheminejad, S., Seifossadat, S.G., and Joorabian, M. "New travelling-wave-based protection algorithm for parallel transmission lines during inter-circuit faults", *IET Gener. Transm. & Distrib.*, **11**(16), pp. 3984–3991 (2017).

33. Hasheminejad, S., Esmaeili, S., and Jazebi, S. "Power quality disturbance classification using S-transform and hidden Markov model", *Elec. Power Comp. Sys.*, **40**(10), pp. 1160–1182 (2012).

34. Meloni, L.G.P., *Learning Discrete Hidden Markov Models*, John Wiley and Sons, *Inc. comput. Appl. Eng. Educ.*, **8**(3), pp. 141–149 (2000).

Biography

Saeid Hasheminejad was born in Kerman, Iran in 1985. He received his BSc degree in Power Electrical Engineering from Iran University of Science and Technology, Tehran, Iran in 2008. Then, he received his MSc and PhD degrees in Power Electrical Engineering from Shahid Bahonar University of Kerman and Shahid Chamran University of Ahvaz in 2011 and 2016, respectively. He is currently working at the Department of Electrical and Computer Engineering as an Assistant Professor at the graduate University of Advanced Technology, Kerman, Iran. His research interests include the signal processing, power quality, and power system protection.